Available online at www.sciencedirect.com
SCIENCE DIRECT®
PERGAMON
Polyhedron 22 (2003) 473–482
POLYHEDRON
www.elsevier.com/locate/poly

Ab-initio studies of cyclic phosphazine systems $(NPX_2)_n$. A study of the structure and bonding in such systems and a search for model systems for the polymer

Mark Enlow

Department of Chemistry, University of New Mexico, Albuquerque, NM 87131, USA

Received 19 August 2002; accepted 19 November 2002

Abstract

Ab-initio molecular orbital calculations were carried out for a series of phosphazine compounds, $(NPX_2)_n$, X = H, F, Cl, and Br, $n = 2$ through 6, in order to study the electronic structure of such compounds and explore their use as model compounds for the bulk polymer. Calculations were carried out at the Hartree–Fock level of theory, using all-electron triple-zeta plus polarization basis sets for all atoms. Full geometry optimizations followed by frequency calculations were performed. Although most species adopted hightly symmetric geometries they were often significantly nonplanar. Optimized geometries are general agreement with geometry's inferred from solution phase IR studies. The geometries of the eight membered and larger rings are very dependent on the identity of X. Ionization energies for this series were calculated using electron propagator theory. Good agreement with experimentally observed values is found. Phosphorus d basis functions appear to be serving as polarization functions rather than being formally involved in bonding.

Keywords: Ab-initio methods; Cyclic phosphazines; Electron propagator methods; Electronic structures; Ionization energies; Vibrational frequencies

1. Introduction

Phosphazine compounds have proven to be an interesting class of inorganic polymers because of a series of unique properties that render them as potentially useful candidates for optical, high-temperature, and ceramic applications. Many of these properties are the result of the P–N backbone in these structures giving rise to unusual chemical bonding characteristics between second and third row elements.

Phosphazine compounds are generally synthesized by reacting phosphorus pentachloride with ammonium chloride under suitable conditions.

$$n\mathrm{PCl_5} + n\mathrm{NH_4Cl} \rightarrow (\mathrm{NPCl_2})_n + 4n\mathrm{HCl}$$

In addition to the bulk polymer, various linear structures and ring structures with n ranging from 3 to 17 have been isolated. Further synthetic steps lead to the partial or complete replacement of Cl atoms with other substituents including but not limited to F, Br, Me, OMe, Ph, and $N(Me)_2$. Four-membered rings are generally not obtained by this procedure but may possibly be obtained from other synthetic routes.

There is some controversy surrounding bonding in phosphazine systems [1]. Formally, the phosphorus nitrogen backbone consists of alternating single and double bonds. However, phosphorus nitrogen bond length in cyclic phosphazines is typically between 1.60 and 1.65 Å, which lies between the typical bond lengths for single and double bonds of 1.76 and 1.57 Å, respectively. The lack of alternating bond lengths in cyclic phosphazine rings have led some to label them as inorganic aromatic molecules. The role that phosphorus d functions play in phosphazines is also somewhat controversial. Phosphorus d_{xy} and d_{yz} functions are often considered to combine with nitrogen p_z functions to form out of plane π bonds which have been described as 'islands of delocalization' about P–N–P ring sections [2].

E-mail address: menlow@ahpcc.unm.edu (M. Enlow).

0277-5387/02/$ - see front matter
PII: S0277-5387(02)01370-0

Theoretical investigation of small phosphazine compounds can lead to further understanding of the structure and bonding in phosphazine systems and can potentially identify species that can serve as model compounds for the bulk polymer.

Several theoretical studies of small linear molecules of the type $O{=}PX_2{-}(N{=}PX_2)_n{-}X$ have been done [3–5]. These calculations reveal alternating P–N bond lengths characteristic of alternating single and double P–N bonds. This is likely a result of the short length of the molecule and the presence of terminal functional groups. Such species are not a likely candidate for a model compound for the polymer.

Other theoretical studies have been done on small cyclic molecules, $(NPX_2)_n$ [6,7]. These investigations have typically been carried out with very modest basis sets and only on the trimeric or tetrameric rings. A more recent publication considered a large number of ring sizes and substituents, and carefully examined the role played by phosphorus d functions, but imposed D_{nh} symmetry on the structures [8]. One of the few works to include post-SCF methods was a study limited to $(NPCl_2)_3$ and similar heterocyclic rings at the MP2/6-31G(d) level of theory [9]. Further calculations on cyclic ring systems are warranted.

Here ab-initio methods are used to explore several small cyclic phosphazine compounds in order to study the nature of bonding in these species and to attempt to identify good model compounds for the bulk polymer. Calculations on the structures $(NPX_2)_n$, X = H, F, Cl, and Br, $n = 2$ through 6, were carried out.

The hydrogen containing species were chosen for study in order to determine the effect of substituents of small size and low electronegativity on the ring backbone, however it should be noted that to the best of our knowledge the hydrogen containing species have not been synthesized as yet.

2. Computational methods

Geometry optimizations were performed at the Hartree-Fock level of theory using the 6-311G(d,p) basis set for all elements. In our suite of programs this specified the 6-311G(d,p) basis set of Pople et al. [10] for the elements H, N, and F; the McLean–Chandler (12s/9p/1d) basis set [11] for Cl; and the 6-311G(d) basis sets of McGrath et al. [12] for Br. Full geometry optimizations were carried out followed by harmonic frequency calculations to characterize the stationary point. The geometries were not constrained to adopt D_{nh} symmetries. Additional property calculations were then performed.

Electron propagator calculations were performed in the OVGF [13,14] approximation using a semidirect algorithm [15,16] that takes advantage of abelian point group symmetry. The same basis set used for geometry optimizations and frequency calculations was used. Core orbitals were omitted from the summations required by this approximation. Iterations on the Dyson equation are performed until electron binding energies are converged to within 0.00001 eV.

Dyson orbitals for an electron detachment from an N-electron state are defined by

$$\phi^{\mathrm{Dyson}}(x_1) = \int \Psi^*_{N-1}(x_2,\ x_3,\ x_4,\ \ldots,\ x_N)\Psi_N(x_1,\ x_2,\ x_3,\ \ldots,\ x_N) \times dx_2 dx_3 dx_4\ \ldots\ dx_N. \quad (1)$$

Propagator programs report electron detachment energies and corresponding pole strengths, p, where

$$p = \int |\phi^{\mathrm{Dyson}}(x_1)|^2\ dx_1. \quad (2)$$

Normalized Dyson orbitals are depicted in plots generated with the program MOLDEN [17]. In the zeroth order propagator, the results of Koopmans theorem are recovered and the pole strengths equal unity. In the OVGF model, correlation contributions are included in the electron binding energies and pole strengths may be less than unity. The closer to unity pole strengths become, the greater the qualitative validity of the Koopmans description of the electron detachment. Dyson orbitals remain proportional to canonical orbitals in the OVGF model.

All calculations were carried out on an IBM SP1 or our IBM RS6000 workstations using a modified version the Gaussian suite of programs [18]. Calculation times ranged from a few minutes to 118 h. Disk space requirements were as high as 17 GB.

3. Results and discussion

3.1. Molecular structures

Geometry optimizations were successfully carried out on the series of molecules $(NPX_2)_n$, X = H, F, Cl, and

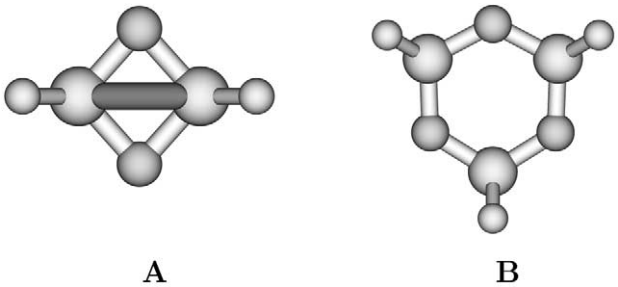

Fig. 1. Representative molecular structures of $(NPX_2)_2$ and $(NPX_2)_3$. (A) D_{2h} $(NPF_2)_2$. (B) D_{3h} $(NPF_2)_3$.

Table 1
Zero point corrected total energies and energies per monomer unit (Au.)

Structure	Energy	Energy/monomer
$(NPH_2)_2$	−792.598513	−396.299256
$(NPH_2)_3$	−1189.020409	−396.340136
$(NPH_2)_4$	−1585.38191	−396.345477
$(NPH_2)_5$	−1981.727284	−396.345456
C_2 $(NPH_2)_6$	−2378.054445	−396.342407
C_i $(NPH_2)_6$	−2378.2427127	−396.373785
$(NPF_2)_2$	−1188.324147	−594.162073
$(NPF_2)_3$	−1782.628913	−594.209637
$(NPF_2)_4$	−2376.863047	−594.215761
'P' C_{2v} $(NPF_2)_5$	−2971.018014	−594.203602
'N' C_{2v} $(NPF_2)_5$	−2971.084979	−594.216995
'P' C_{2v} $(NPF_2)_6$	−3565.28497	−594.214161
C_2 $(NPF_2)_6$	−3565.303515	−594.217252
$(NPCl_2)_2$	−2628.425565	−1314.212782
$(NPCl_2)_3$	−3942.759779	−1314.253259
$(NPCl_2)_4$	−5257.034201	−1314.258550
'P' C_{2v} $(NPCl_2)_5$	−6571.193951	−1314.238790
'NN' C_2 $(NPCl_2)_5$	−6571.298937	−1314.259787
'P' C_{2v} $(NPCl_2)_6$	−7885.525041	−1314.254173
C_2 $(NPCl_2)_6$	−7885.559629	−1314.259938
$(NPBr_2)_2$	−11079.879006	−5539.939503
$(NPBr_2)_3$	−16619.933946	−5539.977982
$(NPBr_2)_4$	−22159.931142	−5539.982785
'P' C_{2v} $(NPBr_2)_5$	−27699.807815	−5539.961563
'NN' C_2 $(NPBr_2)_5$	−27699.918976	−5539.983795
'P' C_{2v} $(NPBr_2)_6$	−33239.861310	−6647.972262
C_2 $(NPBr_2)_6$	−33239.883782	−6647.976756

Br, $n = 2$ through 6. Figs. 1 through 4 illustrate the structure of several of these species. Table 1 summarizes the relative total energies for these molecules as well as the total energy per monomer unit, found by dividing the total energy by n. Table 2 lists selected calculated geometric parameters for the series of structures and experimentally measured geometric data for a number of species as well as the bulk polymer. Optimized geometries are described below, and are compared with geometries inferred from solid and solution phase IR data [19], and are found to be in good agreement with the solution phase geometries.

3.2. $(NPX_2)_2$

Geometry optimization of $(NPX_2)_2$, X = H, F, Cl, and Br, all lead to a trapezoidal D_{2h} conformation. Fig. 1(A) shows a structural plot of $(NPF_2)_2$. All four structures possess a somewhat small P–P distance (2.138 Å in $(NPF_2)_2$), small P–N–P and N–P–N bond angles (see Table 2), and a relatively high energy per monomer value (Table 1) possibly due to a high amount of ring strain in the P–N backbone.

Table 2
Selected calculated and experimental geometric parameters (Å and °)

Structure	P–N	P–X	X–P–X	N–P–N	P–N–P
$(NPH_2)_2$	1.631	1.396	101.4	94.9	85.1
$(NPH_2)_3$	1.591	1.394	101.7	115.8	124.2
$(NPH_2)_4$	1.576	1.394	102.1	120.5	140.3
$(NPH_2)_5$	1.577	1.394	102.5	121.2	141.2
$(NPH_2)_6$	1.579	1.400	102.7	116.8	139.7
$(NPF_2)_2$	1.602	1.522	98.0	96.3	83.7
$(NPF_2)_3$	1.559	1.525	99.1	116.1	123.9
$(NPF_2)_4$	1.537	1.530	99.6	120.0	149.5
$(NPF_2)_5$	1.530	1.533	99.4	119.8	160.2
$(NPF_2)_6$	1.534	1.536	99.3	119.3	154.6
$(NPF_2)_n$ [a]	1.52	1.47	95.	119.	136.
$(NPCl_2)_2$	1.617	1.994	102.9	95.6	84.4
$(NPCl_2)_3$	1.570	2.003	102.7	115.1	124.1
$(NPCl_2)_4$	1.548	2.009	103.1	119.4	147.2
$(NPCl_2)_5$	1.538	2.014	102.8	118.3	158.0
$(NPCl_2)_6$	1.545	2.018	102.7	117.1	155.7
$(NPBr_2)_2$	1.623	2.175	103.8	95.4	84.6
$(NPBr_2)_3$	1.574	2.184	103.6	115.2	124.8
$(NPBr_2)_4$	1.550	2.192	103.8	119.4	150.0
$(NPBr_2)_5$	1.540	2.196	103.5	118.3	162.8
$(NPBr_2)_6$	1.545	2.199	103.3	117.0	150.3

Calculated results are for the most stable conformation, and represent the average values for those species with inequivalent geometric parameters.
[a] Bulk polymer, Ref. [20].

3.3. $(NPX_2)_3$

Geometry optimization of $(NPX_2)_3$, X = H, F, Cl, and Br, all lead to a D_{3h} conformation with a planar, nearly hexagonal P–N backbone. Fig. 1(B) shows a structural plot of $(NPF_2)_3$. Solution phase IR studies of $(NPX_2)_3$ species indicate a D_{3h} geometry, while solid phase $(NPX_2)_3$ structures have been seen to adopt a slightly distorted C_{3v} geometry.

3.4. $(NPX_2)_4$

The optimized geometry of $(NPX_2)_4$ is dependent on the identity of X. When X = F, a D_{4h} conformation with a planar P–N backbone is obtained (Fig. 2(A)). When X = H or Cl, a D_{2d} conformation is obtained. $(NPCl_2)_4$ is shown in Fig. 2(B). Here the phosphorus atoms lie within a plane, while the nitrogen atoms alternate above and below this plane (by approximately 0.4 Å when X = H and 0.2 Å when X = Cl). When X = Br, the optimized geometry is further distorted from D_{4h} by a slight elongation along one axis resulting in a C_{2v} geometry (Fig. 2(C)). This results in a structure with symmetrically inequivalent nitrogen and bromine atoms. Solution phase IR spectra of $(NPF_2)_4$ indicate a D_{4h} geometry, while the chloride and bromide species in the solution phase both indicate a geometry with D_{2d} symmetry. The C_{2v} geometry that was obtained for $(NPBr_2)_4$ is only

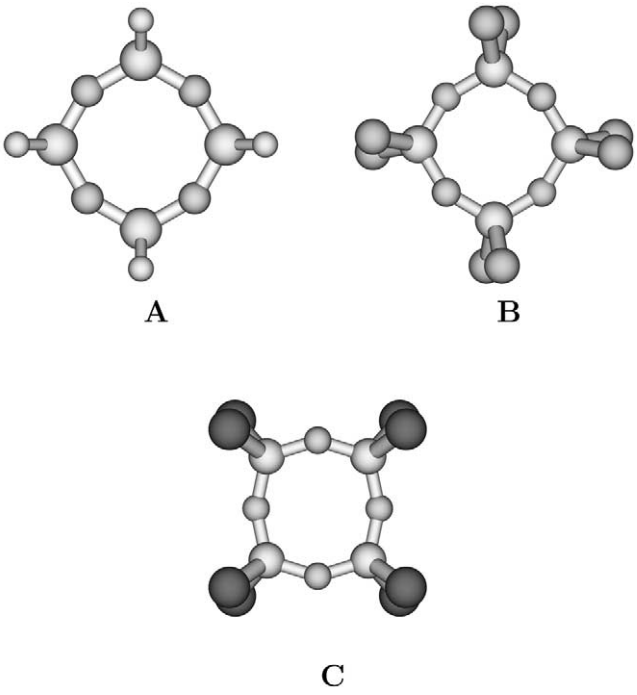

Fig. 2. Representative molecular structures of $(NPX_2)_4$. (A) D_{4h} $(NPF_2)_4$. (B) D_{2d} $(NPCl_2)_4$. (C) C_{2v} $(NPBr_2)_4$.

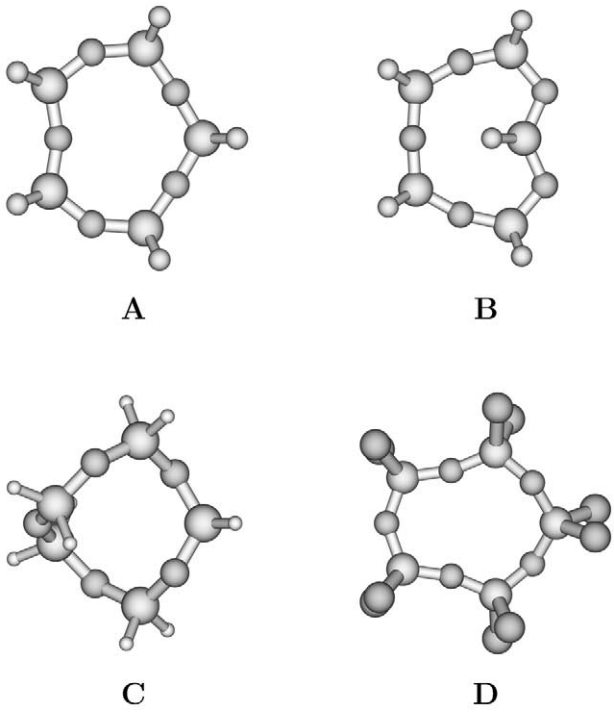

Fig. 3. Representative molecular structures of $(NPX_2)_5$. (A) 'N' C_{2v} $(NPF_2)_5$. (B) 'P' C_{2v} $(NPF_2)_5$. (C) C_2 $(NPH_2)_5$. (D) 'NN' C_2 $(NPCl_2)_5$.

slightly distorted from D_{2d}. It may be the case that the distortion is too small to be inferred from the IR data, or $(NPBr_2)_4$ may revert to a D_{2d} geometry in the solution phase. $(NPX_2)_4$ species in the solid phase have been observed to adopt a variety of conformations having D_{2d}, D_{4h}, C_{2h}, or S_4 geometry depending on the substituent and environment.

3.5. $(NPX_2)_5$

The optimized geometry of $(NPX_2)_5$ is dependent on the identity of X, and in some cases two different minima were identified. The global minima will be described first. When X = H a twisted C_2 conformation with a significantly nonplanar backbone is obtained (Fig. 3(C)). When X = F a C_{2v} conformation is obtained which has a planar P–N backbone (Fig. 3(A)). One of the nitrogen atoms is puckered towards the center of the ring making it somewhat 'heart' shaped. The N–P–N angles remain close to 120° while the P–N–P angles are significantly larger than found in the four member rings (see Table 2). When X = Cl or Br a C_2 conformation with a slightly nonplanar P–N backbone is obtained. $(NPCl_2)_5$ is shown in Fig. 3(D). Here, two of the nitrogen atoms are puckered towards the center of the ring. Here too, the N–P–N angles remain close to 120° while the P–N–P angles are significantly larger than found in the four member rings. Both the Cl and Br structures are very close to a C_{2v} geometry having a planar P–N backbone, the bromine being somewhat closer to planar than the chlorine. Imposing C_{2v} symmetry on these structures resulted in transition states very slightly higher in energy (less than 10^{-6} a.u.) with one imaginary frequency (8 cm^{-1} for the chlorine species and 2 cm^{-1} for the bromine). $(NPX_2)_5$ species in the solid phase have been reported to have a wide variety of geometries of relatively low symmetry.

When X = F, Cl, or Br, a second minimum having C_{2v} symmetry was identified. $(NPF_2)_5$ is shown in Fig. 3(B). Here one of the phosphorus atoms and its two halogen atoms are puckered towards the center of the ring. These conformations were considerably higher in energy than the previously described minima in the case of all three halogens. Attempts to obtain a $(NPH_2)_5$ conformation with a puckered phosphorus atom resulted in a structure with one or more imaginary frequencies corresponding to dihedral rotation about the P–N backbone that would return the molecule to the minimum energy conformation illustrated in Fig. 3(C). It may be the case of the three halogen species that steric crowding between the puckered halogens and the ring prevents dihedral rotation that would return the structure to the global minimum. Evidence of steric crowding can be seen in the P–X bond lengths about the puckering phosphorus atom. When X = F, all P–F bond lengths are approximately equal. When X = Cl or Br, the puckered P–X bond lengths exceed the other P–X bond lengths by approximately 0.1 Å.

3.6. $(NPX_2)_6$

The optimized geometry of $(NPX_2)_6$ is dependent on the identity of X, and in all cases two different minima were identified. The global minima are described first. When X = H a conformation with C_i symmetry with a significantly nonplanar backbone is obtained (Fig. 4(A)). This geometry resembles a S_6 conformation that has been stretched along one axis. When X = F, Cl, or Br, a C_2 conformation is obtained. $(NPF_2)_6$ is shown in Fig. 4(C). Two of the nitrogen atoms are puckered towards the center of the ring. The fluorine containing species has a P–N backbone that is close to planar, while the bromine is somewhat less planar and the chlorine species significantly nonplanar.

For each of the four substituents, a second minimum having C_{2v} symmetry was identified. $(NPF_2)_6$ is shown in Fig. 4(B). Here the P–N backbone is planar, and one of the phosphorus atoms and two nitrogen atoms are puckered towards the center of the ring. These conformations were higher in energy than the minimum described above, although the difference was not as large as the difference between the different minima found for the pentamer compounds. This may indicate that the alternate hexamer conformations posess less ring strain and less steric crowding about the puckered P and X atoms than were present in the alternate pentamer conformations.

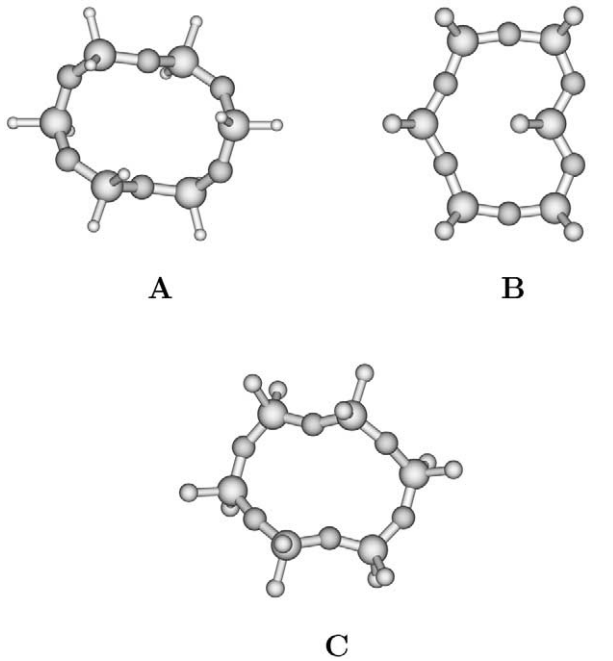

Fig. 4. Representative molecular structures of $(NPX_2)_6$. (A) C_i $(NPH_2)_6$. (B) 'P' C_{2v} $(NPF_2)_6$. (C) C_2 $(NPF_2)_6$.

3.7. Observed trends

The total relative energy per unit generally decreases with increasing ring size. The dimers have a much larger relative total energy per unit, likely due to a high amount of ring strain. Larger ring sizes have more reasonable bond angles. Conformations with phosphorus atoms puckered towards the center of the ring are higher than the more stable conformations. Geometry optimization on initial conformations with nitrogen puckering arangements other than the minima described above were attempted for several of the pentamer and hexamer structures. In all cases the structure would readily convert to the global minima described above. Thus, the P–N–P bond angle appears to be relatively flexible and the barrier to inversion about a nitrogen atom appears to be relatively small. The N–P–N bond angle was found to be more rigid. Most structures tend to assume geometries that maintain N–P–N bond angles near 120° at the expense of P–N–P bond angles. P–N bond lengths decrease with increasing ring size and in the case of the fluorine species appear to be approaching the limit of the bulk polymer.

3.8. Vibrational frequencies

Table 3 presents the calculated vibrational frequencies of $(NPF_2)_3$ as well as experimental data from Raman and gas phase IR spectra. Calculated vibrational frequencies were scaled by a factor of 0.92. The calculated frequencies, estimated IR intensities, and estimated Raman activities are all in good agreement with experimental values. Calculated frequencies differed from experimental values by less than 20 cm^{-1}. The mode at 1306 cm^{-1} is a ring stretching mode of E' symmetry. Ring stretching modes with strong IR absorbtion intensities in the region of 1100–1400 cm^{-1} are characteristic of phosphazine compounds. Experimental studies of phosphazines have shown a gradual increase in ring stretching frequencies up to $n = 5$, followed by a gradual decrease in frequency. This has been interpreted as an indication that rings larger than $n = 5$ adopt less planar conformations than the smaller compounds [19]. Table 4 presents calculated and experimental ring stretching frequencies for the phosphazines studied in this work. The calculated frequency for each molecule that was chosen for presentation in this table was the ring stretching mode that had the highest calculated IR intensity. For the halogen containing species this frequency was often the highest frequency mode in the calculated spectra. The hydrogen containing species had a number of H–P–H bending modes that were much higher in intensity than the ring stretching modes, and were located in the region of 2500–2600 cm^{-1}. The larger and less symmetric species often had several ring stretching modes of similar calculated

Table 3
Calculated and experimental vibrational spectra of $(NPF_2)_3$

Frequency [a]	Symmetry	IR inten [b]	Raman act [b]	Exp IR [c]	Exp Raman [c]
70	E''				
72	A_2''				
228	A_1''				
270	E'		1.8		282(4,dp)
293	E''		2.0		311(4.5,p)
304	A_1'		1.6		342(0.75,dp)
333	E'				
433	E''				
442	A_2'				
456	E'	105	1.4	468(s)	469(1.5,dp)
540	A_2''	140		516(s)	
558	A_1'		2.7		570(2.5,p)
756	A_1'		25.7		743(10,p)
854	E'	543		862(s)	
944	E''		1.2		951(0.75,p)
969	A_2''	737		973(s)	
989	E'				
1022	A_1'		1.9		1012(0.75,p)
1197	A_2'				
1306	E'	1139		1297(vs)	

[a] Calculated frequencies are scaled by 0.92.
[b] Calculated IR intensities and Raman activities less than 5% of the largest intensity or activity are omitted.
[c] Ref. [21].

Table 4
Calculated and experimental ring stretching frequencies (cm^{-1})

Structure	Calculated [a]	Symmetry	Experiment [b]
$(NPH_2)_2$	897	B_{3u}	
$(NPH_2)_3$	1140	E'	
$(NPH_2)_4$	1332	E	
$(NPH_2)_5$	1339	B	
$(NPH_2)_6$	1317	A_u	
$(NPF_2)_2$	1042	B_{3u}	
$(NPF_2)_3$	1306	E'	1297
$(NPF_2)_4$	1461	E_u	1419
$(NPF_2)_5$	1502	B_2	1439
$(NPF_2)_6$	1490	B	1408
$(NPCl_2)_2$	908	B_{3u}	
$(NPCl_2)_3$	1237	E'	1220
$(NPCl_2)_4$	1384	E	1315
$(NPCl_2)_5$	1437	A	1355
$(NPCl_2)_6$	1401	B	1325
$(NPBr_2)_2$	881	B_{3u}	
$(NPBr_2)_3$	1210	E'	1171
$(NPBr_2)_4$	1346	B_1	
$(NPBr_2)_5$	1415	A	
$(NPBr_2)_6$	1385	B	

Calculated results are for the most stable conformation.
[a] Calculated frequencies are scaled by 0.92.
[b] Ref. [19].

intensties, and since calculated IR intensities are often somewhat unreliable it may be that we were not always able to match the correct calculated frequency with the experimental mode of maximal intensity. Nevertheless, agreement between the calculated and experimental frequencies in Table 4 is fair, especially considering that the experimental data was obtained in the solution phase, and the calculated frequencies reproduce the trend of maximal ring stretching frequencies for the $n = 5$ species. The agreement between calculated and experimental frequencies could have been significantly improved by obtaining a new scaling factor through the use of a least-squares fit method.

3.9. Ionization energies

Table 5 presents calculated and experimental values for the ionization energies corresponding to the eight highest occupied orbitals of $(NPF_2)_3$. Molecular orbital contour plots for these orbitals are presented in Fig. 5. Ionization energies estimated from the Hartree-Fock eigenvalues overestimate the ionization energy by

Table 5
Calculated and experimental ionization potentials of $(NPF_2)_3$ (eV)

Orbital	HF eigenvalue	OVGF	Pole strength	Experiment [a]
5 A_2	19.53	17.24	0.91	
6 E_2	19.45	17.09	0.91	
12 E_1	19.26	17.07	0.91	17.2
3 A_1	18.13	15.99	0.91	16.6
10 A_1	17.54	15.38	0.90	15.4
6 A_2	15.18	13.42	0.91	13.1
7 E_2	13.31	11.65	0.91	
13 E_1	13.29	11.51	0.91	11.4

[a] Ref. [23].

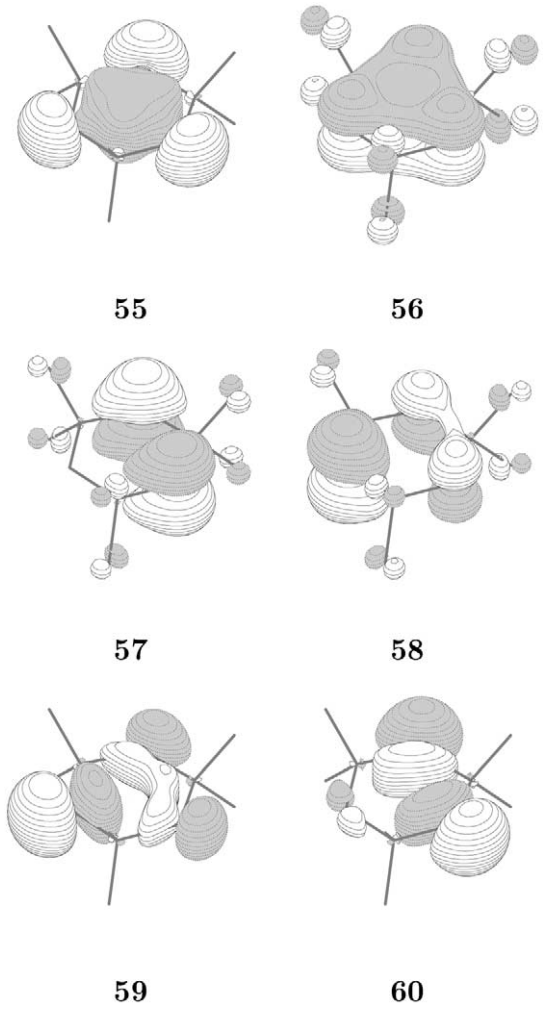

Fig. 5. Molecular orbital contour diagrams for the top six orbitals of $(NPF_2)_3$.

aproximately 2 eV. Ionization energies obtained with the OVGF method fall much closer to the experimental values, most within 0.2 eV. The highest ionization energy corresponds to a molecular orbital of E_1 symmetry, followed by one of E_2 symmetry. These orbitals had OVGF ionization energies of 11.51 and 11.65 eV, respectively. The experimental data cited reports a single peak at 11.4 eV. It is possible the authors were unable to resolve these two ionization potentials in their photoelectron spectra and only reported one energy. This is supported by the fact that peak at 11.4 eV is noticably broader than the other peaks in the spectrum. The next lowest ionization energy corresponded to an orbital of A_2 symmetry, with an OVGF value of 13.42 eV in fair agreement with the experimental value of 13.1 eV.

Table 6 presents the first ionization energies of all species studied in this work. Ionization energies for the majority of the species were calculated using the OVGF method. The high disk space requirements of the OVGF method prevented us from obtaining OVGF results for a few of the larger species. Hartree-Fock eigenvalues and experimental data, where available, are also presented. Agreement between the OVGF and experimental values is good, the OVGF method typically overestimates the ionization energies by a few tenths of an electron volt. For a given ring size, the experimental first ionization energy is seen to increase with the electronegativity of the substituents. In the case of the florine containing species, the first ionization energy is seen to alternate, with odd values of n having higher ionization energies than rings with even values of n. The calculated ionization energies reproduce both of these trends.

3.10. Bonding in phosphazine systems

Many models of the bonding in cyclic phosphazines are based on the assumption that 2p orbitals of the nitrogen and 3d and 4p orbitals of the phosphorus are involved to some degree in π type bonding about P–N backbone, while the 3s and 3p orbitals of the phosphorus are involved in σ bonding with the nitrogen and substituent atoms. Fig. 6 illustrates some of the resonance structures that may be involved in this type of bonding scheme for $(NPF_2)_3$. Structure 6A involves localization of lone pair electrons on the nitrogen atoms and no involvement of phosphorus orbitals in π bonding. Structure 6B and similar resonance structures involve bonding between nitrogen and phosphorus atoms and participation of the phosphorus 3d orbitals. Structure 6C and similar resonance structures again involve π bonding between nitrogen and phosphorus atoms but assume a degree of ionic bonding between phosphorus and substituent atoms. Such structures require little or no contribution from phosphorus 3d orbitals.

Table 7 lists the partial atomic charges obtained from Muliken population analysis for the ring systems studied. For a given ring size, the magnitude of the charges on the P and X centers increases with increasing substituent electronegativity. Also, for any given substituent, the magnitude of the charges on all atoms increases with increasing ring size. Thus bonding between atoms in larger rings also become somewhat more ionic in nature. This increases the ionic nature of the P–X bond and increases the contribution from resonance structures similar to 6C, which would increase the amount ring π bonding and favor geometries with shorter P–N bond lengths and more planar P–N backbones.

These trends are in good agreement with our results, especially for the optimized structures of the tetramers and larger rings, where the geometry was found to be very dependent on the identity of the substituent. For a given substituent, P–N bond lengths were found to decrease with ring size. For any given ring size, the P–N bond lengths and ring stretching frequencies were found

Table 6
Calculated and experimental first ionization potentials (eV)

Structure	Symmetry	HF eigenvalue	OVGF	Pole strength	Experiment
$(NPH_2)_2$	B_{3g}	10.20	9.02	0.91	
$(NPH_2)_3$	A_2''	10.42	9.51	0.91	
$(NPH_2)_4$	B_2	9.99	8.81	0.90	
$(NPH_2)_5$	B	9.98	8.80	0.90	
$(NPH_2)_6$	A_g	10.15	8.96	0.90	
$(NPF_2)_2$	B_{3g}	11.78	10.33	0.91	
$(NPF_2)_3$	E'	13.29	11.51	0.91	11.58 [a], 11.4 [b]
$(NPF_2)_4$	B_{1g}	12.08	10.32	0.91	10.7 [b]
$(NPF_2)_5$	B_2	12.48	10.67	0.90	11.4 [b]
$(NPF_2)_6$	B	12.48			10.9 [b]
$(NPCl_2)_2$	B_{3g}	11.26	9.69	0.90	
$(NPCl_2)_3$	E''	12.10	10.56	0.90	10.11 [a], 10.26 [b], 10.3 [c]
$(NPCl_2)_4$	B_2	11.53	9.79	0.90	9.80 [b]
$(NPCl_2)_5$	B	11.84			9.83 [b]
$(NPCl_2)_6$	B	11.91			9.81 [b]
$(NPBr_2)_2$	B_{3g}	10.88	9.37	0.90	
$(NPBr_2)_3$	E''	11.32	10.01	0.90	9.62 [a], 9.6 [c]
$(NPBr_2)_4$	A_1	11.11	9.51	0.90	9.2 [c]
$(NPBr_2)_5$	B	11.31			
$(NPBr_2)_6$	B	11.29			

Calculated results are for the most stable conformation.
[a] Ref. [22].
[b] Ref. [23].
[c] Ref. [24].

to decrease with increasing electronegativity of the substituent. The fluorine substituted phosphazines showed the greatest tendency to form structures with planar P–N backbones, while the hydrogen-substituted phosphazines assumed geometries with the most nonplanar P–N backbones. The chlorine and bromine species, having electronegativities between those of hydrogen and fluorine, formed structures somewhat between the hydrogen and fluorine species in terms of planarity of the P–N backbone. However, the bromine species tended be closer to planar than the chlorine species. It is possible that the large bromine substituents (and to a lesser extent the chlorine substituents) limit the amount of nonplanar deformation that can occur due to steric crowding about the phosphorus centers. Trends in geometries observed for the larger ring sizes can therefore be seen as a tradeoff between the electronegativity and the size of the substituent atoms.

The inclusion of d functions (polarization functions) is a common way of improving the accuracy of ab-initio calculations. Although the inclusion of d functions in typical organic molecules often produces minimal improvement, the inclusion of phosphorus d functions in phosphazine systems markedly improves the results. Calculated geometric, frequencies, and ionization energies show a dramatic improvement with the inclusion of d functions. In several cases, geometric optimization without d functions led to a structure of a different point group than was obtained from optimizations with d functions. In those cases it was the geometry obtained with the inclusion of d functions that agreed with experimental observations.

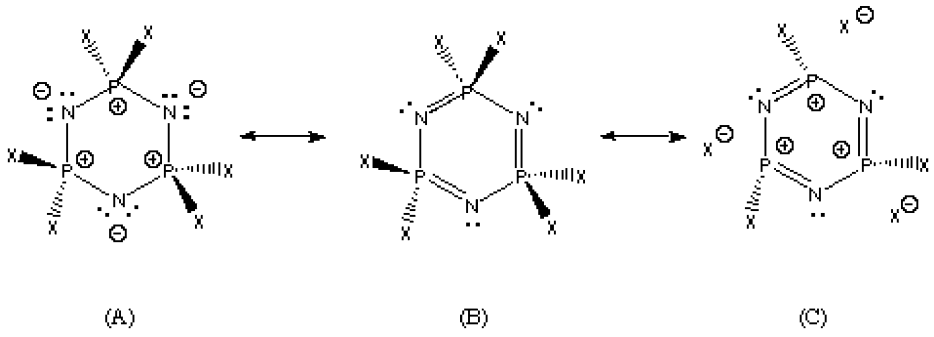

Fig. 6. Some of the possible resonance structures for $(NPF_2)_3$ according to the bonding scheme discussed in the text.

Table 7
Partial atomic charges and gross d-rbital populations (for the phosphorus atoms only) obtained from Muliken population analysis

Species	P	N	X	P d-orbital population
$(NPH_2)_2$	+1.082	−0.916	−0.083	0.387
$(NPH_2)_3$	+1.217	−1.042	−0.087	0.397
$(NPH_2)_4$	+1.242	−1.054	−0.094	0.408
$(NPH_2)_5$	+1.238	−1.054	−0.092	0.407
$(NPH_2)_6$	+1.236	−1.055	−0.090	0.406
$(NPF_2)_2$	+1.602	−0.850	−0.375	0.630
$(NPF_2)_3$	+1.745	−0.976	−0.384	0.627
$(NPF_2)_4$	+1.788	−1.012	−0.387	0.641
$(NPF_2)_5$	+1.793	−1.005	−0.394	0.651
$(NPF_2)_6$	+1.801	−1.011	−0.393	0.638
$(NPCl_2)_2$	+1.186	−0.839	−0.174	0.494
$(NPCl_2)_3$	+1.338	−0.968	−0.185	0.498
$(NPCl_2)_4$	+1.390	−0.991	−0.199	0.515
$(NPCl_2)_5$	+1.405	−0.985	−0.210	0.523
$(NPCl_2)_6$	+1.409	−0.989	−0.212	0.518
$(NPBr_2)_2$	+1.083	−0.822	−0.131	0.437
$(NPBr_2)_3$	+1.216	−0.949	−0.134	0.445
$(NPBr_2)_4$	+1.265	−0.969	−0.148	0.465
$(NPBr_2)_5$	+1.277	−0.961	−0.158	0.473
$(NPBr_2)_6$	+1.281	−0.956	−0.162	0.463

Results are for the most stable conformation, and represent the averaged values for those species with inequivalent atoms.

The magnitude of the role played by phosphorus d orbitals can be estimated from the Muliken population analysis. Table 7 contains the gross d-orbital population for the phosphorus atoms as obtained from a Muliken population analysis. This represents the approximate number of electrons that occupy d basis functions on the phosphorus atoms, including electrons involved in σ-bonding and nonbonding electrons as well as those involved in bonding. This quantity ranges from a low of 0.39 in the hydrogen dimer to a high of 0.65 in the fluorine pentamer. The gross d-orbital population generally increases with increasing ring size and with increasing substituent electronegativity. For those species where two different minima were identified, there was little difference in d-orbital populations even when there was a large difference in the degree of planarity between the two conformations. In all cases the quantity remains less than what would be expected if phosphorus d orbitals were formally populated and involved in π bonding with the nitrogen p orbitals.

Thus it appears that phosphorus d functions are being used to provide subtle corrections to the molecular orbitals and can be identified as polarization functions rather than being formally involved in bonding, and contributions from resonance structures similar to 6B appear to be minimal.

The small size and high symmetry of $(NPF_2)_3$ makes it a convenient choice for illustration and discussion of the several highest molecular orbitals. Fig. 5 shows orbital contour plots of the six highest occupied orbitals of $(NPF_2)_3$. The top six orbitals are all dominated by contributions from nitrogen 2p orbitals, with small contributions from fluorine p orbitals and almost no contribution from phosphorus centered orbitals. The HOMO orbital is a degenerate E set composed of p orbitals perpendicular to the plane of the P–N backbone. Although the phase of the orbitals indicates an anti-bonding interaction, the large distance between the nitrogen atoms indicates that the overlap is small and the interaction weak. The HOMO-4 orbital again involves nitrogen p orbitals perpendicular to the ring in a bonding interaction. The remaining three of the top six orbitals are dominated by contributions from nitrogen *p* orbitals in the plane of the P–N backbone to form weakly bonding molecular orbitals. Thus the top six molecular orbitals appear to be nitrogen-centered and primarily nonbonding or weakly bonding in nature, which seems to agree with resonance structures similar to 6A. Although the ordering of orbitals varied, the top six orbitals of the other three trimers studied were qualitatively similar to those of $(NPF_2)_3$. Similarly, the top several molecular orbitals of ring systems other than the trimers were found to be dominated by nitrogen centered p orbitals. Tetramer and larger ring systems have larger N–P–N bond angles which would result in even weaker interactions between nitrogen p orbitals.

4. Conclusion

Optimized geometries retain a high amount of symmetry in most cases until the hexamer is reached. The P–N backbone tends to assume geometries in which the N–P–N bond angles remain near 120°. The P–N–P bond angle appears to be more flexible and varies to a much larger extent. Tetramer and larger systems assume differing geometries depending on the identity of the substituent, and can be rationalized in terms of the electronegativity and size of the substituent.

The inclusion of d type basis functions greatly improve the accuracy of calculated physical properties by providing suble improvements to the molecular orbitals, however phosphorus d orbitals do not appear to be formally involved in or bonding.

Unlike the linear species studied elsewhere, the symmetric cyclic species exhibit little or no variation in P–N bond length. Several geometric and physical properties appear to be approaching the value for the polymer as ring size is increased. Physical properties such as vibrational frequencies and ionization energies can be calculated with good accuracy.

Dimer and trimer systems are characterized by small P–N–P and N–P–N angles when compared with experimental values for the polymer, which makes them unattractive as models for the polymer. Hexamer compounds adopt conformations of relatively low

symmetry with makes their computational cost high. Tetramer and pentamer compounds may provide the best compromise between computational cost and coorelation with the bulk polymer.

Acknowledgements

Dr J.V. Ortiz and V.G. Zakrewski of Kansas State University, and Dr E. Walters of The University of New Mexico provided extensive advice for this project. In addition the authors would like to thank the Albuquerque High Performance Computing Center (AHPCC) for the use of their computational resources. This work was funded in part by grants from the National Science Foundation and the Petroleum Research Fund.

References

[1] For example, see: P. Wisian-Nelson, in: R.B. King (Ed.), Encyclopedia of Inorganic Chemistry, vol. 6 (and references therein), Wiley, New York, 1995, p. 3371.
[2] M.J.S. Dewar, E.A.C. Lucken, M.A. Whitehead, J. Chem. Soc. (1960) 2423.
[3] M. Breza, S. Biskupic, J. Mol. Struct. 332 (1995) 277.
[4] M. Breza, J. Mol. Struct. 429 (1998) 111.
[5] M. Breza, J. Mol. Struct. 454 (1998) 77.
[6] K.F. Ferris, C.B. Duke, Int. J. Quantum Chem. 23 (1989) 397.
[7] M. Breza, S. Biskupic, J. Mol. Struct. 309 (1994) 305.
[8] M. Breza, Polyhedron 19 (2000) 389.
[9] R. Jaeger, M. Debowski, I. Manners, G.J. Vancso, Inorg. Chem. 38 (1998) 1153.
[10] R.K. Krishnan, J.S. Binkley, R.S. Seeger, J.A. Pople, J. Chem. Phys. 72 (1980) 650.
[11] A.D. McLean, G.S. Chandler, J. Chem. Phys. 72 (1980) 5639.
[12] (a) R.C. Binning, Jr., L.A. Curtis, J. Comp. Chem. 11 (1990) 1206; (b) M.P. McGrath, L. Radom, J. Chem. Phys. 94 (1991) 511.
[13] L.S. Cederbaum, J. Phys. B 8 (1975) 290.
[14] W. von Niessen, J. Schirmer, L.S. Cederbaum, Comput. Phys. Rep. 1 (1984) 57.
[15] V.G. Zakrzewski, J.V. Ortiz, Int. J. Quant. Chem. Quant. Chem. Symp. 28 (1994) 23.
[16] V.G. Zakrzewski, J.V. Ortiz, Int. J. Quantum Chem. 53 (1995) 583.
[17] G. Schaftenaar, MOLDEN, CAOS/CAMM Center, The Netherlands, 1991.
[18] M.J. Frisch, G.W. Trucks, H.B. Schlegel, P.M.W. Gill, B.G. Johnson, M.A. Robb, J.R. Cheeseman, T. Keith, G.A. Petersson, J.A. Montgomery, K. Raghavachari, M.A. Al-Laham, V.G. Zakrzewski, J.V. Ortiz, J.B. Foresman, J. Cioslowski, B.B. Stefanov, A. Nanayakkara, M. Challacombe, C.Y. Peng, P.Y. Ayala, W. Chen, M.W. Wong, J.L. Andres, E.S. Replogle, R. Gomperts, R.L. Martin, D.J. Fox, J.S. Binkley, D.J. Defrees, J. Baker, J.P. Stewart, M. Head-Gordon, C. Gonzalez, J.A. Pople, GAUSSIAN-94, Revision D.3, Gaussian, Inc., Pittsburgh, PA, 1995.
[19] D.E.C. Corbridge, The Structural Chemistry of Phosphorus, Elsevier Scientific, London, 1974, p. 333.
[20] H.R. Allcock, R.L. Kugel, E.G. Stroh, Inorg. Chem. 11 (1972) 1121.
[21] A.C. Chapman, N.L. Paddock, J. Chem. Soc. (1961) 635.
[22] P. Clare, D.B. Sowerby, J. Inorg. Nucl. Chem. 43 (1981) 744.
[23] G.R. Branton, C.E. Brion, D.C. Frost, K.A.R. Mitchell, N.L. Paddock, J. Chem. Soc., Sect. A (1970) 151.
[24] G.E. Coxon, T.F. Palmer, D.B. Sowerby, J. Chem. Soc. A (1969) 358.